Title

Triggering Receptor Expressed on Myeloid Cells 2 Alleviated Sevoflurane-Induced Developmental Neurotoxicity via Microglial Pruning of Dendritic Spines in the CA1 Region of the Hippocampus

Authors

Deng, Li

Song, Shao-Yong

Zhao, Wei-Ming

et al.

Publication Date

2024-07-29

DOI

10.1007/s12264-024-01260-9

Neurosci. Bull.
https://doi.org/10.1007/s12264-024-01260-9

www.neurosci.cn
www.springer.com/12264

ORIGINAL ARTICLE

Triggering Receptor Expressed on Myeloid Cells 2 Alleviated Sevoflurane-Induced Developmental Neurotoxicity via Microglial Pruning of Dendritic Spines in the CA1 Region of the Hippocampus

Li Deng[1,2] · Shao-Yong Song[1,3] · Wei-Ming Zhao[1,2] · Xiao-Wen Meng[1,2] · Hong Liu[4] · Qing Zheng[5] · Ke Peng[1,2] · Fu-Hai Ji[1,2]

Received: 9 September 2023 / Accepted: 14 March 2024

Abstract Sevoflurane induces developmental neurotoxicity in mice; however, the underlying mechanisms remain unclear. Triggering receptor expressed on myeloid cells 2 (TREM2) is essential for microglia-mediated synaptic refinement during the early stages of brain development. We explored the effects of TREM2 on dendritic spine pruning during sevoflurane-induced developmental neurotoxicity in mice. Mice were anaesthetized with sevoflurane on postnatal days 6, 8, and 10. Behavioral performance was assessed using the open field test and Morris water maze test. Genetic knockdown of TREM2 and overexpression of TREM2 by stereotaxic injection were used for mechanistic experiments. Western blotting, immunofluorescence, electron microscopy, three-dimensional reconstruction, Golgi staining, and whole-cell patch-clamp recordings were performed. Sevoflurane exposures upregulated the protein expression of TREM2, increased microglia-mediated pruning of dendritic spines, and reduced synaptic multiplicity and excitability of CA1 neurons. TREM2 genetic knockdown significantly decreased dendritic spine pruning, and partially aggravated neuronal morphological abnormalities and cognitive impairments in sevoflurane-treated mice. In contrast, TREM2 overexpression enhanced microglia-mediated pruning of dendritic spines and rescued neuronal morphological abnormalities and cognitive dysfunction. TREM2 exerts a protective role against neurocognitive impairments in mice after neonatal exposures to sevoflurane by enhancing microglia-mediated pruning of dendritic spines in CA1 neurons. This provides a potential therapeutic target in the prevention of sevoflurane-induced developmental neurotoxicity.

Keywords CA1 neurons · Dendritic spines · Developmental neurotoxicity · Microglia · Sevoflurane · TREM2

Li Deng and Shao-Yong Song contributed equally to this work.

Supplementary Information The online version contains supplementary material available at https://doi.org/10.1007/s12264-024-01260-9.

✉ Ke Peng
pengke0422@163.com

✉ Fu-Hai Ji
jifuhaisuda@163.com

1 Department of Anaesthesiology, The First Affiliated Hospital of Soochow University, Suzhou 215006, China

2 Institute of Anaesthesiology, Soochow University, Suzhou 215006, China

3 Department of Anaesthesiology, Dushu Lake Hospital Affiliated of Soochow University, Suzhou 215000, China

4 Department of Anaesthesiology and Pain Medicine, University of California Davis Health, Sacramento, CA, USA

5 Center for Molecular Imaging and Nuclear Medicine, Collaborative Innovation Center of Radiation Medicine of Jiangsu Higher Education, State Key Laboratory of Radiation Medicine and Protection, School for Radiological and Interdisciplinary Sciences (RAD-X), Suzhou Medical College of Soochow University, Suzhou 215006, China

Introduction

Multiple anaesthetic exposures in early life induce abnormal central nervous system development and neurobehavioral impairment, also known as anaesthetic-induced developmental neurotoxicity (AIDN) [1]. The possibility of neurodevelopmental disorders in paediatric anaesthesia has led to increasing concerns [2–5]. However, the neurobiological mechanisms underlying AIDN remain unclear.

Published online: 29 July 2024

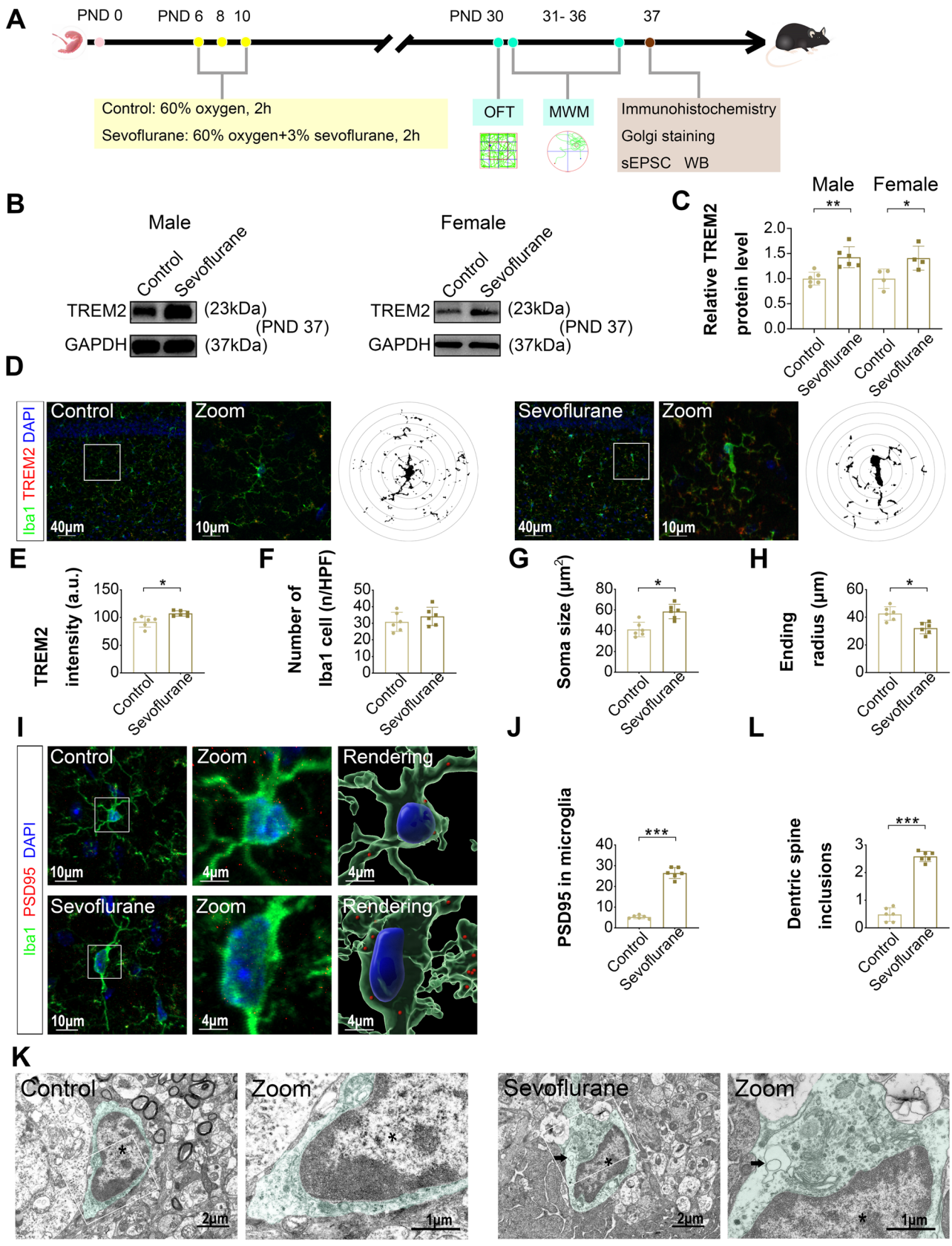
A
PND 0
PND 6 8 10
PND 30
31- 36
37
Control: 60% oxygen, 2h
Sevoflurane: 60% oxygen+3% sevoflurane, 2h
OFT
MWM
Immunohistochemistry
Golgi staining
sEPSC WB
B
Male
Female
Control
Sevoflurane
TREM2 (23kDa)
GAPDH (37kDa)
(PND 37)
C
Male Female
Relative TREM2 protein level
D
Iba1 TREM2 DAPI
Control
Zoom
Sevoflurane
40μm
10μm
E
TREM2 intensity (a.u.)
F
Number of Iba1 cell (n/HPF)
G
Soma size (μm²)
H
Ending radius (μm)
I
Iba1 PSD95 DAPI
Rendering
4μm
J
PSD95 in microglia
L
Dentric spine inclusions
K
2μm
1μm

◂**Fig. 1** Neonatal sevoflurane exposures upregulated TREM2 expression, activated microglia, and increased microglial engulfment of dendritic spines in mice hippocampus. **A** Schematic of experimental design. **B** Representative bands of TREM2 protein expression in the control and sevoflurane mice of both sexes. **C** Quantification of TREM2 protein expression (male: $n = 6$; female: $n = 4$; $P = 0.909$ for male vs female). **D** Immunofluorescence staining of colocalization of TREM2 with microglial marker Iba1 and Sholl analysis of microglia morphology in the control and sevoflurane groups. **E–H** Quantification of TREM2 intensity, number of microglia, soma size, and the ending radius of microglia in the 2 groups ($n = 6$). **I** Representative images and 3D surface rendering of $Iba1^+$ microglia (green) containing $PSD95^+$ puncta (red) in the control and sevoflurane groups. **J** Quantification of $PSD95^+$ puncta in microglia in the 2 groups ($n = 6$). **K** Electron micrograph of microglia in the control and sevoflurane groups. Asterisks denote the nucleus and the cytoplasm is pseudocolored green. Arrowheads designate engulfed dendritic spine elements. **L** Quantification of dendritic spine inclusions in microglia in the 2 groups ($n = 6$). Data are mean ± SD. Unpaired *t*-test; $^{*}P < 0.05$, $^{**}P < 0.01$, $^{***}P < 0.001$. PND, postnatal day; OFT, open field test; MWM, Morris water maze; WB, western blot; sEPSC, spontaneous excitatory postsynaptic current.

Postnatal synaptogenesis is a highly dynamic process regulated by concurrent synapse formation and elimination. Studies have suggested that neonatal anaesthetic exposures impaired dendritic growth and synaptogenesis [6, 7]. Microglial cells are the resident immune cells of the brain. Microglia-mediated synaptic pruning is a complex process that regulates synapse formation, supernumerary synapse elimination, and appropriate synapse connections [8, 9]. Triggering receptor expressed on myeloid cell 2 (TREM2), a microglial innate immune receptor, is essential for microglia-mediated synaptic refinement, microglial activation, and elimination of defective synapses in the hippocampus [10].

Sevoflurane is the most widely used anaesthetic for paediatric anaesthesia. In our previous study, snRNA-seq data illustrated the upregulation of TREM2 expression in the mouse hippocampus after early-life sevoflurane exposures, and microglia remained in a state related to synaptic pruning [11]. Based on these findings, we hypothesized that TREM2 plays a crucial role in the pathophysiology of AIDN. We designed this experimental study to investigate the regulatory effect of TREM2 on microglial pruning of dendritic spines in the mouse hippocampus after multiple neonatal exposures to sevoflurane.

Materials and Methods

Mice

The animal experiments were approved by the Institutional Animal Care and Use Committee of Soochow University, China (protocol number: 202105A0320). C57BL/6J and heterozygous *Trem2* knockout (KO) mice (*Trem2*$^{-/+}$) were purchased from Jiangsu GemPharmatech Co. Ltd. (*Trem2* Cas9-KO, stock number: T003754). The line was maintained by successive backcrossing of heterozygotes. Both female and male mice were used in this study. All mice were housed under controlled conditions (5 mice per cage, 12-h light/dark cycle, 22–26 °C, and 40%–50% humidity), with free access to standard chow and water.

Anaesthesia, Randomisation, and Blinding

The offspring mice were randomly allocated to the sevoflurane or control groups by online simple randomisation (https://www.randomizer.org/) and concealment using opaque sealed envelopes. The animal model was described previously (details available in the Supplemental file) [11]. For harvesting tissue samples, mice were anaesthetized using ketamine (100 mg/kg) and xylazine (20 mg/kg) and euthanized by cervical dislocation [12]. The research investigators who performed the following experiments and statistical analyses were blinded to the allocation.

Stereotaxic Injection of Lentiviruses

Recombinant lentiviruses (LV-TREM2) and lentiviral vectors (LV-con) were synthesized by BrainVTA (Wuhan, China). On postnatal day (PND) 14, the mice were anaesthetized and fixed on a stereotactic frame. Lentiviral particles were injected into the CA1 region of each hemisphere (bregma coordinates: 1.7 mm anteroposterior, 1.2 mm mediolateral, and 1.5 mm dorsoventral). Three weeks later, the protein expression of TREM2 in the hippocampus was measured by western blotting.

Behavioral Studies

Behavioral tests were conducted on PND 30–36 (Fig. 1A). On PND 30, the open field test (OFT) was used to assess general behavioral performance and anxiety responses. The Morris water maze (MWM) test was used to evaluate spatial learning and memory on PND 31–36. The details of OFT and MWM are available in the Supplemental file.

Western Blotting

Total protein from the hippocampus was isolated using tissue lysis buffer, separated by sodium dodecyl sulfate-polyacrylamide gel electrophoresis, and transferred to polyvinylidene fluoride membranes. The membranes were incubated with primary antibodies, followed by incubation with peroxidase-conjugated secondary antibodies (details available in the Supplemental file). Protein bands were visualized using an enhanced chemiluminescence detection solution, and densitometric quantification was performed using the ImageJ software (National Institutes of Health, Bethesda, MD, USA).

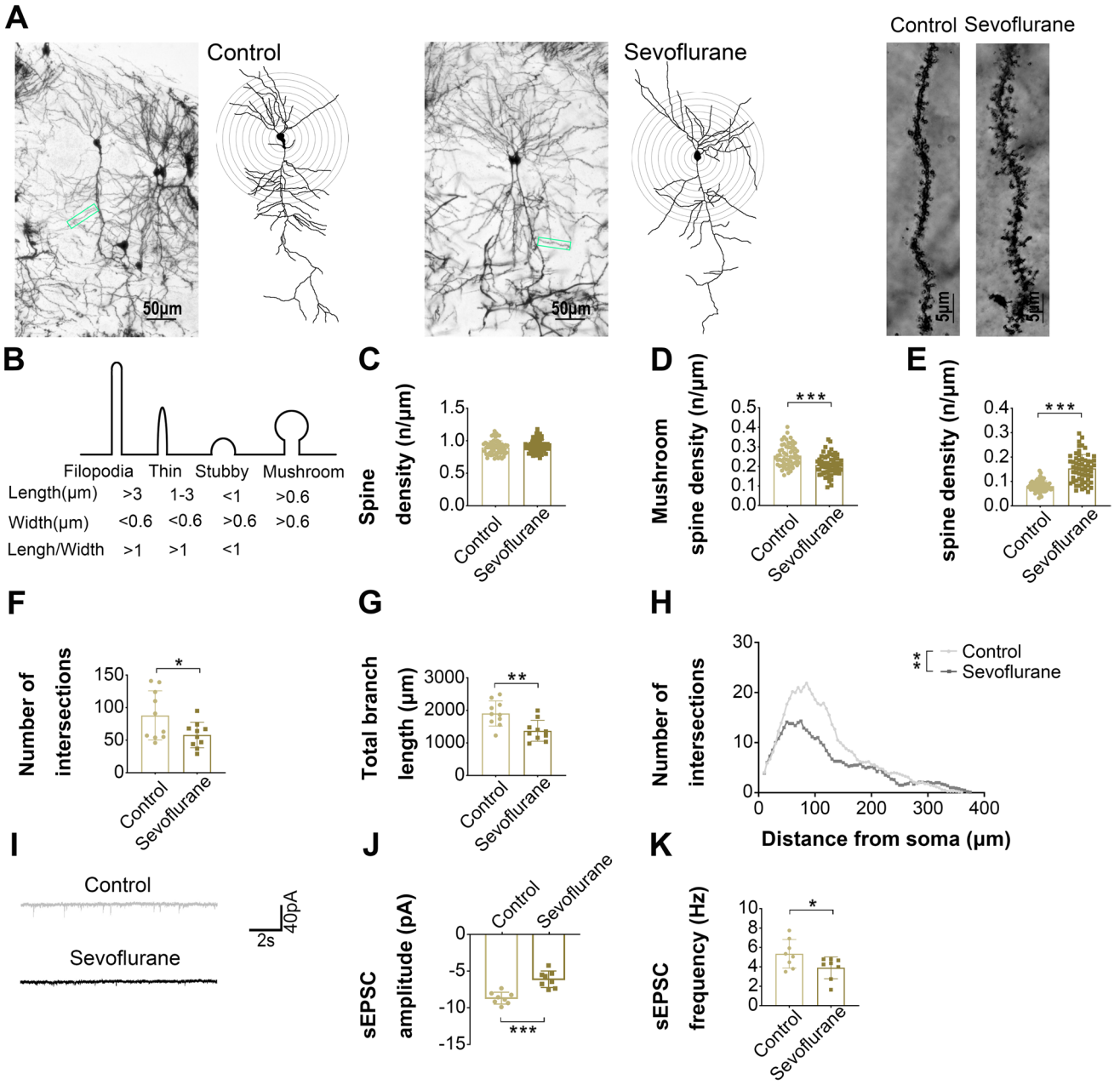

Fig. 2 Neonatal sevoflurane exposures impaired morphology and excitability of hippocampal CA1 pyramidal neurons. **A** Representative Golgi staining images of CA1 pyramidal neurons and dendritic spines in the control and sevoflurane groups. **B** Four distinct types of dendritic spines based on measurements of spine length (base to tip) and width (at the widest point). **C–E** The density of total, mushroom, and filopodia spines in the control and sevoflurane groups (n = 60). **F–G** Number of intersections and total branch length of dendrites in the 2 groups (n = 10). **H** Number of intersections along the dendrites at all distances from the soma of CA1 neurons in the 2 groups (n = 10; F = 12.194, P = 0.030). **I** Representative traces of sEPSCs of whole-cell patch-clamp recordings from CA1 pyramidal neurons in the control and sevoflurane groups. **J–K** Quantification of sEPSCs amplitude and frequency in the control and sevoflurane groups (n = 8). Data are mean ± SD. Unpaired t-test or two-way repeated-measure analysis of variance; $^{*}P < 0.05$, $^{**}P < 0.01$, $^{***}P < 0.001$. sEPSC, spontaneous excitatory postsynaptic current.

Immunofluorescence

Brain samples were dissected, post-fixed overnight in 4% paraformaldehyde at 4 °C, and transferred to 30% sucrose for 72 h. After embedding the brain tissues with the optimal cutting temperature compound (Sakura Finetek, Torrance, CA, USA), 30mm tissue sections were prepared using a Leica cryostat (Leica, Wetzlar, Germany). Subsequently, the sections were incubated with primary and secondary antibodies (details available in Supplemental file). Sections were

counterstained and mounted in Vectashield antifade mounting medium with 4′,6-diamidino-2-phenylindole (DAPI) (Vector Laboratories, Burlingame, CA, USA). Fluorescent images were captured using a confocal microscope (Zeiss, Oberkochen, Germany) and analyzed using ImageJ.

Microglial Engulfment

Microglial engulfment was analyzed using IMARIS software (Bitplane, Zürich, Switzerland). First, the three-dimensional surface of the microglia was reconstructed. Next, $PSD95^+$ puncta were reconstructed using the IMARIS ''Spots'' function. We used the IMARIS MATLAB-based (MathWorks) plugin ''Split into Surface Objects'' to assess the number of $PSD95^+$ puncta entirely within the microglial surface.

Electron Microscopy

Hippocampal sections were selected for electron microscopy. The CA1 area was cut into 2mm×2mm pieces. Sections were fixed with a mixture of 2% paraformaldehyde, 2.5% glutaraldehyde, and 2 mM $CaCl_2$ in 0.1 M cacodylate buffer (pH 7.4) for 4 h. The specimens were dehydrated in a 30% and 50% acetone series, followed by overnight dehydration with 70% acetone-saturated uranium acetate. The specimens were further dehydrated using a graded series of ethanol at resolutions of 89, 90, and 100%. Next, the sections were embedded in Durcupan water-soluble resin (Head Biotechnology, Beijing, China) between ACLAR embedding films (Head Biotechnology) for 72 h at 55 °C. The sections were imaged using an electron microscope (Hitachi, Tokyo, Japan). Under electron microscopy, the characteristics of microglia included their size (3–6 μm), electron-dense cytoplasm, and bean-shaped nuclei with pockets of compact heterochromatin nets [13]. Filamentous or thread-like actin filaments and the only organelle of smooth endoplasmic reticulum were the hallmark features for identifying dendritic spines [14].

Golgi Staining

Brain samples were treated according to the instructions of the Golgi Stain™ Kit (FD Neuro Technologies, Columbia, MD, USA). Coronal sections (100 μm in thickness) including hippocampal structures were prepared using a freezing microtome (Leica). Golgi-stained images were captured using a microscope (Olympus, Tokyo, Japan) and composited through the extended depth of field function. The Image J software and relevant plugins (http://www.imagescience.org/meijering/software/neuronj/; http://fiji.sc/Sholl_Analysis) were used for image processing and morphological analyses. Spine densities were analyzed by counting the number of spines along 10–60 μm segments on the secondary apical dendritic branches in the CA1 region and 50–100 μm segments on the secondary branches in the DG region.

Electrophysiology

Brain samples were quickly removed and placed in artificial cerebrospinal fluid containing 95% oxygen and 5% carbon dioxide. Coronal sections (400 μm in thickness) of the hippocampus were prepared using a vibration microtome (VY1200S, Leica). The slices were incubated in NMDG ACSF (saturated with $95\%O_2/5\%CO_2$ to provide a stable pH and continuous oxygenation) at 37 °C for 30 min at room temperature for 1 h. Brain slices were then transferred to the recording tank. The recording electrode was filled with artificial cerebrospinal fluid and the resistance was maintained at 3–6 mV. The recording electrode was placed on the stratum radiata of CA1. Small excitatory postsynaptic potential (sEPSP) amplitudes and frequencies were recorded for 4 min.

Statistical Analysis

All statistical analyses were performed using SPSS version 21.0 (IBM, Armonk, NY, USA). The normal distribution of data was checked using the Shapiro–Wilk test. Data are presented as mean ± standard deviation (SD) and were analyzed using unpaired *t*-test, one-way ANOVA followed by Tukey's post hoc test, or two-way repeated-measure ANOVA followed by Bonferroni's post hoc test. There were no missing data and no data were excluded from the statistical analyses. Between-group differences were considered statistically significant if the two-sided $P < 0.05$.

Results

Activation of TREM2 and Microglia-Mediated Synaptic Pruning in the Mouse *Hippocampus* after Multiple Neonatal Exposures to Sevoflurane

A schematic diagram of the experimental procedure is shown in Fig. 1A. Our previous hippocampal snRNA-seq data revealed that sevoflurane increased the expression of *TREM2* in microglia. Western blotting confirmed that sevoflurane exposure, when compared with the control, upregulated hippocampal TREM2 protein expression on PND 37 in both male and female mice (Fig. 1B, C), without significant sex-related difference.

Our previous snRNA-seq data showed that microglia remained in a state associated with synaptic pruning

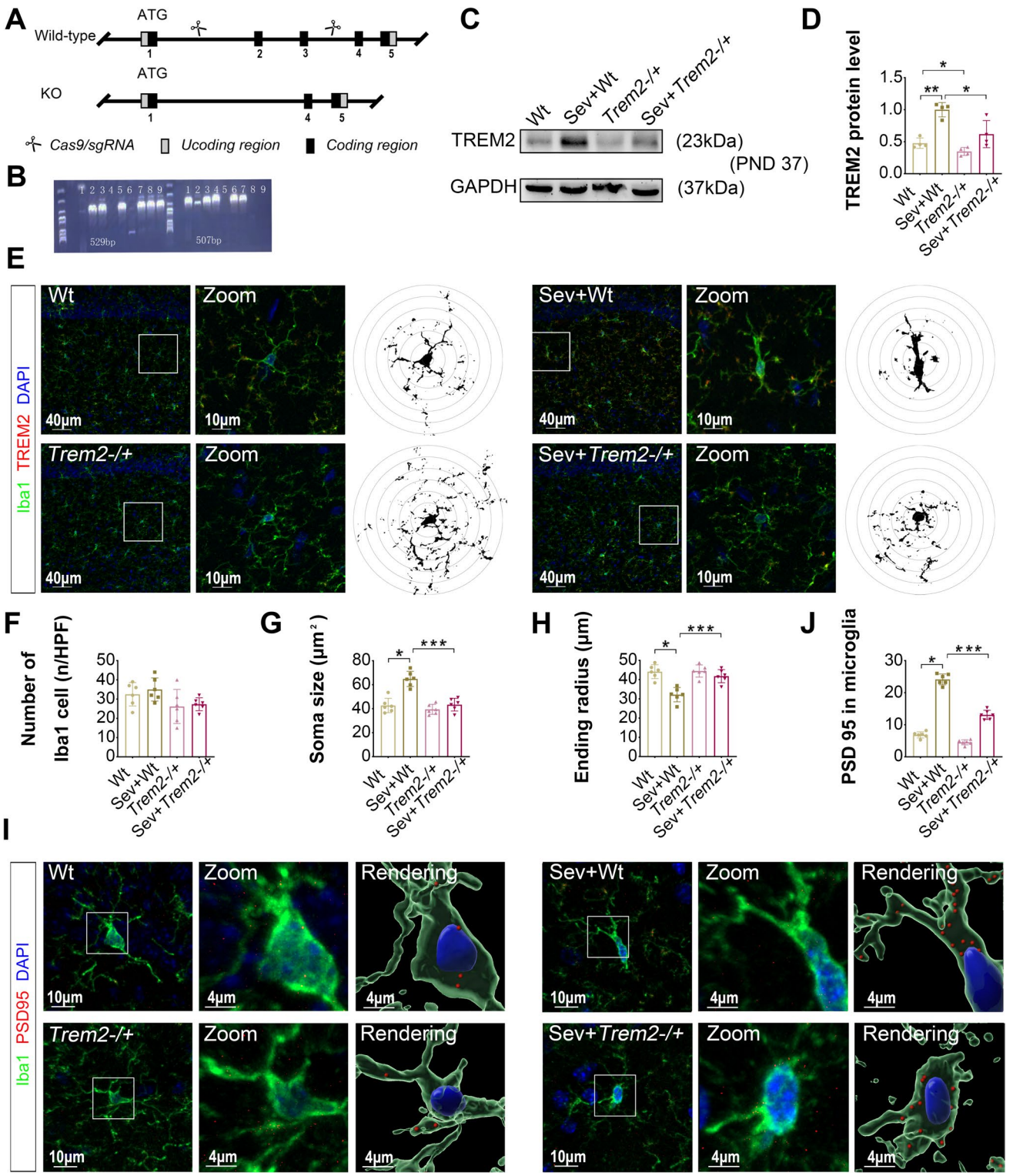

following sevoflurane exposure. Hence, we investigated microglia-mediated synaptic pruning in the CA1 region (a crucial brain area for learning and memory) using immunofluorescent staining for TREM2 and Iba1 (Fig. 1D). The results showed that sevoflurane upregulated the expression of TREM2 (Fig. 1E), without affecting the number of microglia (Fig. 1F). Moreover, sevoflurane induced microglial activation in the CA1 region as the soma became larger (Fig. 1G) and the ending radius of the process was shortened (Fig. 1H). We also found that Iba1 was co-localized with the

◂**Fig. 3** Genetic knockdown of TREM2 inhibited sevoflurane-induced microglia activation and engulfment of dendritic spines in mice hippocampus. **A** Schematic for TREM2 knock-out. **B** Electrophoretic bands of TREM2 gene expression in wild-type (507 bp only; mice 1, 4, and 6), homozygous knock-out (529 bp only; mice 5, 8, and 9), heterozygous knock-out ($Trem2^{-/+}$) mice (both 529 and 507 bp; mice 3 and 7). **C** Representative bands of TREM2 protein expression in the hippocampus of wild-type and $Trem2^{-/+}$ mice with or without sevoflurane treatment on PND 37. **D** Quantification of TREM2 protein expression among the 4 groups ($n = 4$). **E** Immunofluorescence staining of colocalization of TREM2 with microglial marker Iba1 and Sholl analysis of microglia morphology in the 4 groups. **F–H** Quantification of number of microglia, soma size, and the ending radius of microglial processes in the 4 groups ($n = 6$). **I** Representative images and 3D surface rendering of $Iba1^+$ microglia (green) containing $PSD95^+$ puncta (red) in the 4 groups. **J** Quantification of $PSD95^+$ puncta in microglia in the 4 groups ($n = 6$). Data are mean ± SD. One-way analysis of variance followed by Tukey post hoc test. $^*P < 0.05$, $^{**}P < 0.01$, $^{***}P < 0.001$.

microglia-restricted marker TMEM119 (Fig. S1A, B), and TREM2 was almost exclusively expressed on $TMEM119^+$ microglial cells (Fig. S1C).

Immunofluorescence and three-dimensional reconstruction results showed that immunoreactive puncta of postsynaptic density 95 (PSD95), a marker of postsynaptic components, colocalized with Iba1-labeled microglial processes in the hippocampus (Fig. 1I). Quantification revealed a significantly higher number of PSD95 puncta in the sevoflurane-treated group (Fig. 1J). Electron micrographs identified the microglia (Fig. 1K), showing that the sevoflurane group contained an increased number of phagosomes with dendritic spines per cell (Fig. 1L).

Abnormal Morphology and Excitability of CA1 Pyramidal Neurons after Sevoflurane Exposures

To determine whether sevoflurane exposure affected the morphology of CA1 neurons, we evaluated the dendritic spines on the secondary apical dendritic branches in the CA1 region by Golgi staining on PND 37 (Fig. 2A). Among the 4 types of dendritic spines, mushroom spines were the most stable, whereas filopodia spines were the most motile (Fig. 2B). Sevoflurane did not change the total spine density of CA1 neurons (Fig. 2C); however, it significantly decreased the mushroom spine density (Fig. 2D) and increased the filopodia spine density (Fig. 2E) on apical dendrites.

Golgi staining also revealed that sevoflurane reduced the number of intersections (Fig. 2F) and the total branch length in the dendritic tree of CA1 neurons (Fig. 2G). Sholl analysis showed significantly reduced dendritic branching at all distances from the soma in the sevoflurane group (Fig. 2H). To further assess the changes in synaptic multiplicity after sevoflurane exposure, we measured sEPSCs in CA1 neurons on PND 37 (Fig. 2I). The results show that sevoflurane led to a significant decrease in the amplitude (Fig. 2J) and frequency of sEPSCs (Fig. 2K).

Next, we analyzed the dendritic spines of CA1 neurons and TREM2 protein expression on PNDs 10–25 to explore the effects of sevoflurane in the early phase. The sevoflurane group showed significant increases in densities and a decrease in mushroom spine density on both PND 10 (Fig. S2A–D) and 20 (Fig. S2E–H). Western blotting revealed that the protein expression of TREM2 increased from PND 20 (Fig. S2I, J), indicating that the upregulation of TREM2 occurred later than the morphological changes in dendritic spines.

The hippocampal dentate gyrus (DG) is involved in learning and memory. Thus, we measured the microglia and neurons in the DG region in the control and sevoflurane groups. No between-group differences were detected in TREM2 expression, number of microglia, soma size, or ending radius of the process (Fig. S3A–E). The two groups had similar characteristics of dendritic spines in DG neurons (Fig. S3F–I). No differences were observed in the intersections, total dendritic length, or Sholl results between the two groups (Fig. S3J–L).

Decreased Microglia-Mediated Engulfment of Dendritic Spines in the CA1 Region by Downregulation of TREM2 Expression

To investigate the role of TREM2 in sevoflurane exposures, we used *Trem2* heterozygous KO ($Trem2^{-/+}$) mice and control littermates (Fig. 3A, B). Compared with wild-type (Wt) mice, hippocampal TREM2 protein expression was downregulated in $Trem2^{-/+}$ mice before and after sevoflurane exposure (Fig. 3C, D).

We found that downregulation of TREM2 expression did not change the number of microglia in $Trem2^{-/+}$ mice (Fig. 3E, F) but reduced microglial activation after sevoflurane exposure (Fig. 3G, H). Measurement of engulfment capacity also revealed that microglia in the CA1 region of $Trem2^{-/+}$ mice displayed significantly reduced engulfment of PSD95 compared to that in Wt mice after sevoflurane exposure (Fig. 3I, J).

Deterioration of Morphological Abnormalities in the CA1 Neurons and Cognitive Impairment by Downregulation of TREM2 Expression

Golgi staining indicated no differences in the density of different types of dendritic spines, number of intersections, total dendritic length, and dendritic branches between the $Trem2^{-/+}$ and Wt mice (Fig. 4A–G). However, sevoflurane exposures led to significant

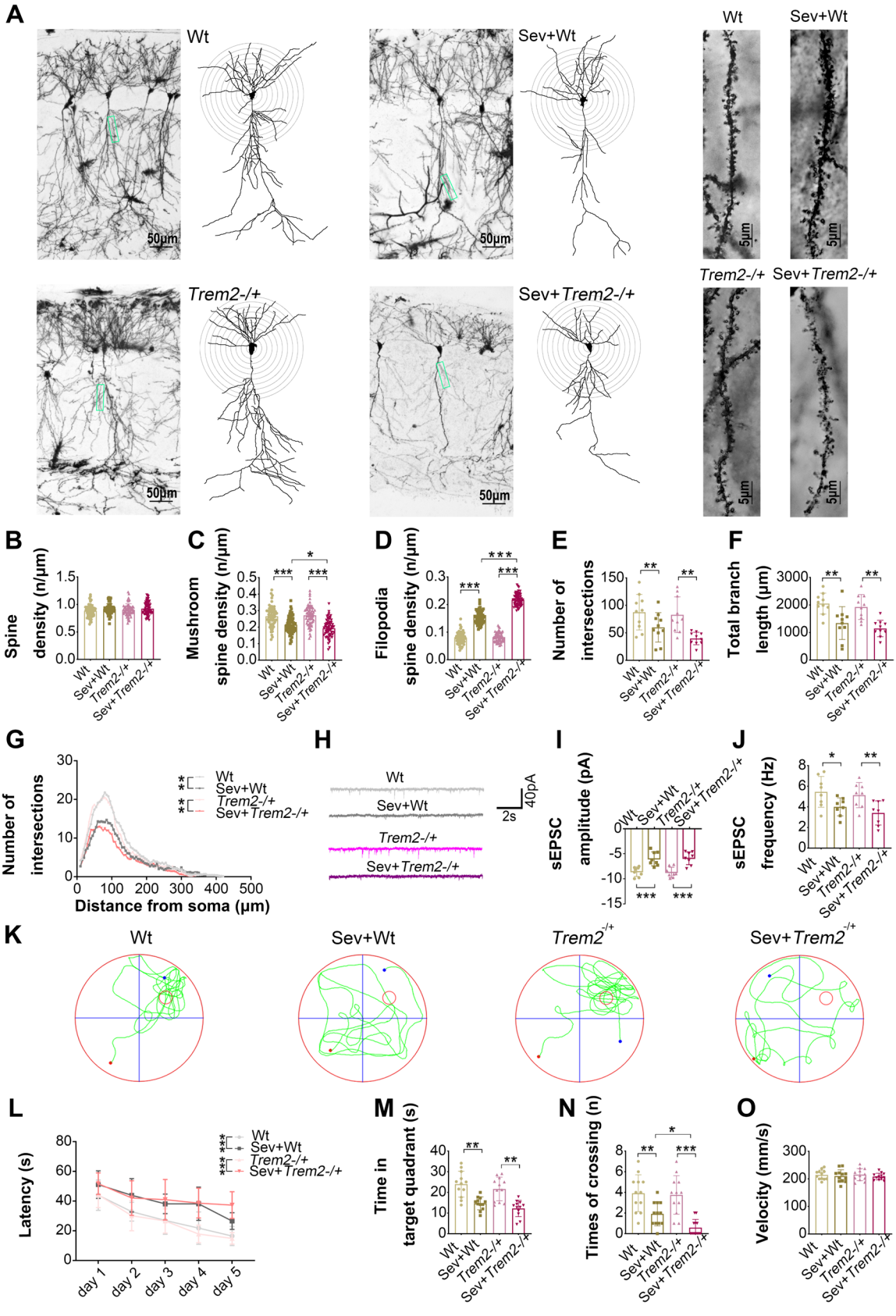
A
Wt
Sev+Wt
Trem2-/+
Sev+Trem2-/+
50μm
5μm
B
Spine density (n/μm)
C
Mushroom spine density (n/μm)
D
Filopodia spine density (n/μm)
E
Number of intersections
F
Total branch length (μm)
G
Number of intersections
Distance from soma (μm)
H
40pA
2s
I
sEPSC amplitude (pA)
J
sEPSC frequency (Hz)
K
Trem2-/+
Sev+Trem2-/+
L
Latency (s)
day 1
day 2
day 3
day 4
day 5
M
Time in target quadrant (s)
N
Times of crossing (n)
O
Velocity (mm/s)

◂**Fig. 4** TREM2 knockdown aggravated sevoflurane-induced morphological abnormalities of hippocampal CA1 pyramidal neurons and exacerbated cognitive impairment. **A** Representative Golgi staining images of CA1 pyramidal neurons and dendritic spines in the wild-type and Trem2$^{-/+}$ mice with or without sevoflurane treatment. **B–D** The density of total, mushroom, and filopodia spines in the 4 groups (n = 60). **E–F** Number of intersections and total branch length of dendrites in the 4 groups (n = 10). **G** Number of intersections along the dendrites at all distances from the soma of CA1 neurons in the 4 groups (n = 10, F = 6.416, P = 0.010). **H** Representative traces of sEPSCs of whole-cell patch-clamp recordings from CA1 neurons in the 4 groups. **I–J** Quantification of sEPSCs amplitude and frequency in the 4 groups (n = 8). **K** Representative moving traces of the 4 groups on the testing stage of MWM. (**L**) Escape latency of the 4 groups in the 5 days on the training stage of MWM (n = 12, F = 32.22 $P < 0.001$). **M–O** Time spent in the fourth quadrant, platform-crossing times, and swimming speed of the 4 groups on the testing stage of MWM (n = 12). Data are mean ± SD. One-way analysis of variance followed by Tukey post hoc test, or two-way repeated-measure analysis of variance followed by Bonferroni post hoc test. $^{*}P < 0.05$, $^{**}P < 0.01$, $^{***}P < 0.001$. MWM, Morris water maze; sEPSC, spontaneous excitatory postsynaptic current.

morphological changes in the CA1 neurons of *Trem2*$^{-/+}$ mice. The Sev+*Trem2*$^{-/+}$ group displayed fewer mushroom dendritic spines (Fig. 4C) and more filopodia dendritic spines (Fig. 4D) than those in the Sev+Wt group. However, between-group differences were not found in the number of intersections (Fig. 4E) and the total dendritic length (Fig. 4F). The degree of dendrite branching at all distances from the soma was similar between Wt and *Trem2*$^{-/+}$ mice before and after sevoflurane exposure (Fig. 4G).

Whole-cell patch-clamp recordings revealed that *Trem2*$^{-/+}$ mice showed no differences in the amplitude and frequency of sEPSCs (Fig. 4H–J) compared with Wt mice. The Sev+*Trem2*$^{-/+}$ group had reduced amplitude (Fig. 4I) and frequency (Fig. 4J) compared with the *Trem2*$^{-/+}$ group. There were no significant differences between the Sev+Wt and Sev+*Trem2*$^{-/+}$ groups.

Mice were tested using the OFT on PND 30 (Fig. S4A–E), showing comparable velocity in the entire arena, frequency in the central region, and duration and moving distance in the central region among all four groups. These results suggested that the performance changes in the MWM were not a result of reduced locomotor ability or anxiety. The MWM test was performed on PND 31-36 (Fig. 4K). Compared with the Wt group, the escape latency of the Sev+Wt group was markedly increased (Fig. 4L), and the time spent in the fourth quadrant (Fig. 4M) and platform crossing times (Fig. 4N) were significantly reduced. The *Trem2*$^{-/+}$ and Wt mice performed similarly in the MWM test. Compared with the Sev+Wt group, the escape latency did not change in the Sev+*Trem2*$^{-/+}$ group (Fig. 4L), but the platform crossing times were significantly decreased in the Sev+*Trem2*$^{-/+}$ group (Fig. 4N). There were no significant differences in swimming speed among the four groups (Fig. 4O).

Increased Microglia-Mediated Engulfment of Dendritic Spines in the CA1 Region by TREM2 Overexpression

To confirm the role of TREM2, mice were locally injected with LV-TREM2 or LV-con into the CA1 area of the hippocampus on PND 14 (Fig. 5A, B). The efficacy of lentiviral transduction was examined by western blotting on PND 37 (Fig. 5C). TREM2 protein expression was higher in LV-TREM2 mice than in LV-con mice and after sevoflurane exposure (Fig. 5D).

Immunofluorescence analysis indicated that LV-TREM2 administration contributed to microglial activation (Fig. 5E–H) and enhanced synaptic pruning (Fig. 5I, J). After sevoflurane exposures, the Sev+LV-TREM2 group displayed a more dramatic change in the soma size (Fig. 5G) and synaptic engulfment of PSD95 (Fig. 5J).

Amelioration of Morphological Abnormalities in the CA1 Neurons and Cognitive Impairment by TREM2 Overexpression

Golgi staining shows the morphological characteristics of the LV-con, Sev+LV-con, LV-TREM2, and Sev+LV-TREM2 groups (Fig. 6A). The four groups had comparable spine densities (Fig. 6B). Sevoflurane exposure in LV-con mice reduced the density of mushroom spines (Fig. 6C) and increased the number of filopodia spines (Fig. 6D). The number of intersections (Fig. 6E), total dendritic length (Fig. 6F), and degree of dendrite branching (Fig. 6G) decreased at all distances from the soma.

TREM2 overexpression attenuated these morphological changes. LV-TREM2 injection not only increased the density of mushroom spines (Fig. 6C) but also prevented the increase in filopodia spines (Fig. 6D) in the Sev+LV-TREM2 group relative to those in the Sev+LV-con group. TREM2 overexpression also significantly increased the total dendritic length (Fig. 6F) and the degree of dendrite branching at all distances from the soma (Fig. 6G).

Whole-cell patch-clamp recordings were performed. Compared with the LV-con group, the LV-TREM2 group showed no difference in the amplitude and frequency of sEPSCs in hippocampal CA1 neurons (Fig. 6H–J). After sevoflurane exposure, the amplitude (Fig. 6I) and frequency of sEPSCs (Fig. 6J) were significantly reduced in LV-con mice, whereas these changes were not observed in LV-TREM2 mice. TREM2 overexpression reversed sevoflurane-induced reductions in the amplitude and frequency of sEPSCs.

In the OFT, neither LV-TREM2 injection nor sevoflurane exposure induced changes in locomotor ability or anxiety

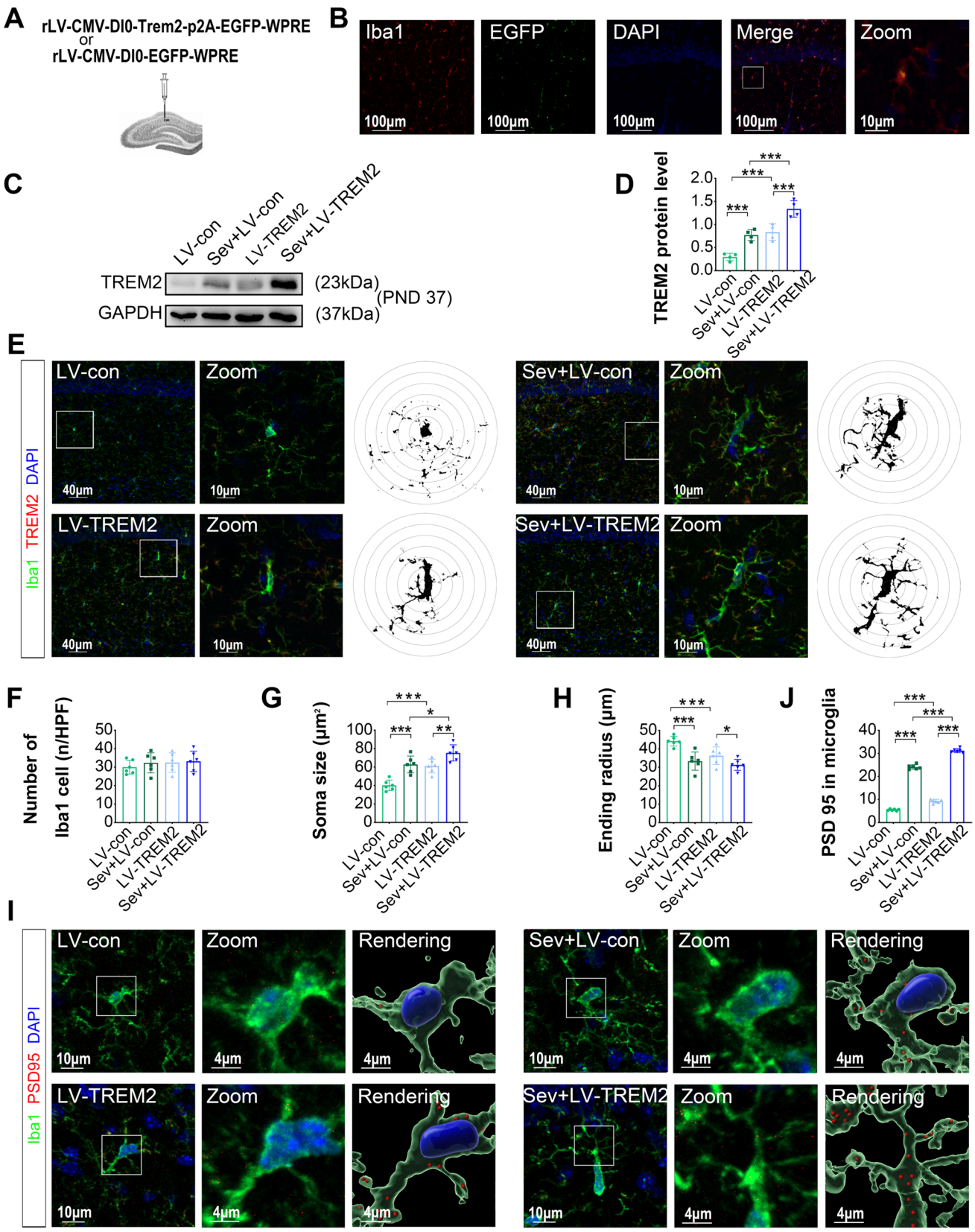
A
rLV-CMV-DI0-Trem2-p2A-EGFP-WPRE
or
rLV-CMV-DI0-EGFP-WPRE
B
Iba1
EGFP
DAPI
Merge
Zoom
100μm
10μm
C
LV-con
Sev+LV-con
LV-TREM2
Sev+LV-TREM2
TREM2
(23kDa)
GAPDH
(37kDa)
(PND 37)
D
TREM2 protein level
E
Iba1 TREM2 DAPI
LV-con
Zoom
Sev+LV-con
LV-TREM2
Sev+LV-TREM2
40μm
10μm
F
Number of Iba1 cell (n/HPF)
G
Soma size (μm²)
H
Ending radius (μm)
J
PSD 95 in microglia
I
Iba1 PSD95 DAPI
Rendering
4μm

◂**Fig. 5** Overexpression of TREM2 enhanced sevoflurane-induced microglia activation and engulfment of dendritic spines in mice hippocampus. **A** Microinjection of a lentivirus (LV-TREM2) or a control vehicle (LV-con). **B** Immunofluorescence images showing the expression of EGFP with colocalization of $Iba1^+$ microglia in the CA1 region. **C** Representative bands of TREM2 protein expression in the hippocampus of LV-con and LV-TREM2 mice with or without sevoflurane treatment on PND 37. **D** Quantification of TREM2 protein expression among the 4 groups (n = 4). **E** Immunofluorescence staining of colocalization of TREM2 with microglial marker Iba1 and Sholl analysis of microglia morphology in the 4 groups. **F-H** Quantification of the number of microglia, soma size, and the ending radius of microglial processes in the 4 groups (n = 6). **I** Representative images and 3D surface rendering of $Iba1^+$ microglia (green) containing $PSD95^+$ puncta (red) in the 4 groups. **J** Quantification of $PSD95^+$ puncta in microglia in the 4 groups (n = 6). Data are mean ± SD. One-way analysis of variance followed by Tukey post hoc test. $^*P < 0.05$, $^{**}P < 0.01$, $^{***}P < 0.001$. EGFP, enhanced green fluorescent protein.

(Fig. S4F–J). The MWM showed that the Sev+LV-con group had prolonged escape latency (Fig. 6L), less time spent in the fourth quadrant (Fig. 6M), and reduced number of platform crossings (Fig. 6N) compared with that in the LV-con group. TREM2 overexpression rescued sevoflurane-induced behavioral changes, as evidenced by less time spent searching for the platform (Fig. 6L), more time spent in the fourth quadrant (Fig. 6M), and a higher number of platform crossings (Fig. 6N). Swimming speed was similar among the four groups (Fig. 6O).

Discussion

This study provides new mechanistic insights into sevoflurane-induced developmental neurotoxicity. We observed increased TREM2 expression and microglia-mediated synaptic pruning in the mouse hippocampi after multiple exposures to sevoflurane. Genetic knockdown of TREM2 inhibited sevoflurane-induced microglial activation and engulfment of dendritic spines, partially deteriorated the morphological abnormalities of CA1 neurons, and partially exacerbated neurobehavioral dysfunction. In contrast, TREM2 overexpression facilitated microglia-mediated engulfment of dendritic spines, rescued the synaptic multiplicity of neurons, and ameliorated neurobehavioral abnormalities. Therefore, our results demonstrated the causal role of TREM2 in microglia in sevoflurane-induced developmental neurotoxicity.

Millions of children worldwide undergo general anaesthesia annually. A growing number of studies have suggested a relationship between volatile anaesthetics and adverse neurocognitive outcomes in young populations. Synaptic abnormalities are considered to be a critical mechanism of AIDN [15]. The peak synaptogenic period in humans occurs between the third trimester of pregnancy and the first few years of postnatal life. This period occurs between the second and fourth postnatal weeks in mice [16]. In the present study, we administered sevoflurane on PNDs 6, 8, and 10 to establish the AIDN mouse model. This period is equivalent to ages 6–12 months in humans. Recent experimental studies have suggested that anaesthetics interfere with synaptogenesis and lead to the fundamental rewiring of neural circuits during brain development; these effects may be lifelong [17].

Microglia play a crucial role in the maturation of synaptic multiplicity. Microglia engulf supernumerary synapses in the developing brain and regulate the dynamics of synaptic connections throughout life [18]. Microglia-mediated synaptic pruning is a highly regulated process that may be activated in vulnerable brain regions in several disease models [19, 20]. Dendritic spines receive the most excitatory inputs to pyramidal cells. Spine heads contain hundreds of proteins, including NMDA, AMPA, and scaffolding proteins such as PSD95. Our three-dimensional reconstruction data showed that most PSD95 puncta co-localized with Iba1, and PSD95 puncta density increased after sevoflurane treatment. Thus, the present study revealed enhanced synaptic engulfment after sevoflurane exposures on PND 37.

TREM2 is a major pathology-induced immune signaling hub that interacts with a wide array of ligands (bacterial products, DNA, lipoproteins, and phospholipids) [21, 22]. TREM2 is essential for microglia-mediated synaptic refinement during the early stages of brain development, which maintains the number and activation of microglia and promotes spine elimination [23]. Mice lacking TREM2 regulation display abnormal dendritic spine pruning during development [10]. Our previous data from the snRNA-seq analysis and western blotting confirmed that TREM2 was significantly upregulated in this model [11]. In the current study, we found that TREM2 knockdown reduced microglia-mediated phagocytic activity with a significantly lower PSD95 puncta. In contrast, TREM2 overexpression promoted the microglia-mediated engulfment of dendritic spines. There is a wide range of ligands of TREM2, including free or cell membrane-bound anionic molecules such as bacterial byproducts, DNA, lipoproteins, and various surface phospholipids [21]. Some ligands are physiologically present, such as cellular debris, lipoproteins (low-density lipoprotein), apolipoproteins, and phosphatidylserine [24, 25]. These endogenous ligands act as an "eat-me" signal and prompt the production of TREM2. Based on these, we assumed that damaged neural cells exposed to sevoflurane initiated a cellular signaling cascade and promoted the production of TREM2, which may serve as a potential molecular mechanism underlying the effect of sevoflurane on the expression of TREM2.

Dendritic spine abnormalities are the most consistent anatomical correlates of altered cognitive function in various neurological disorders [26]. Most excitatory synaptic

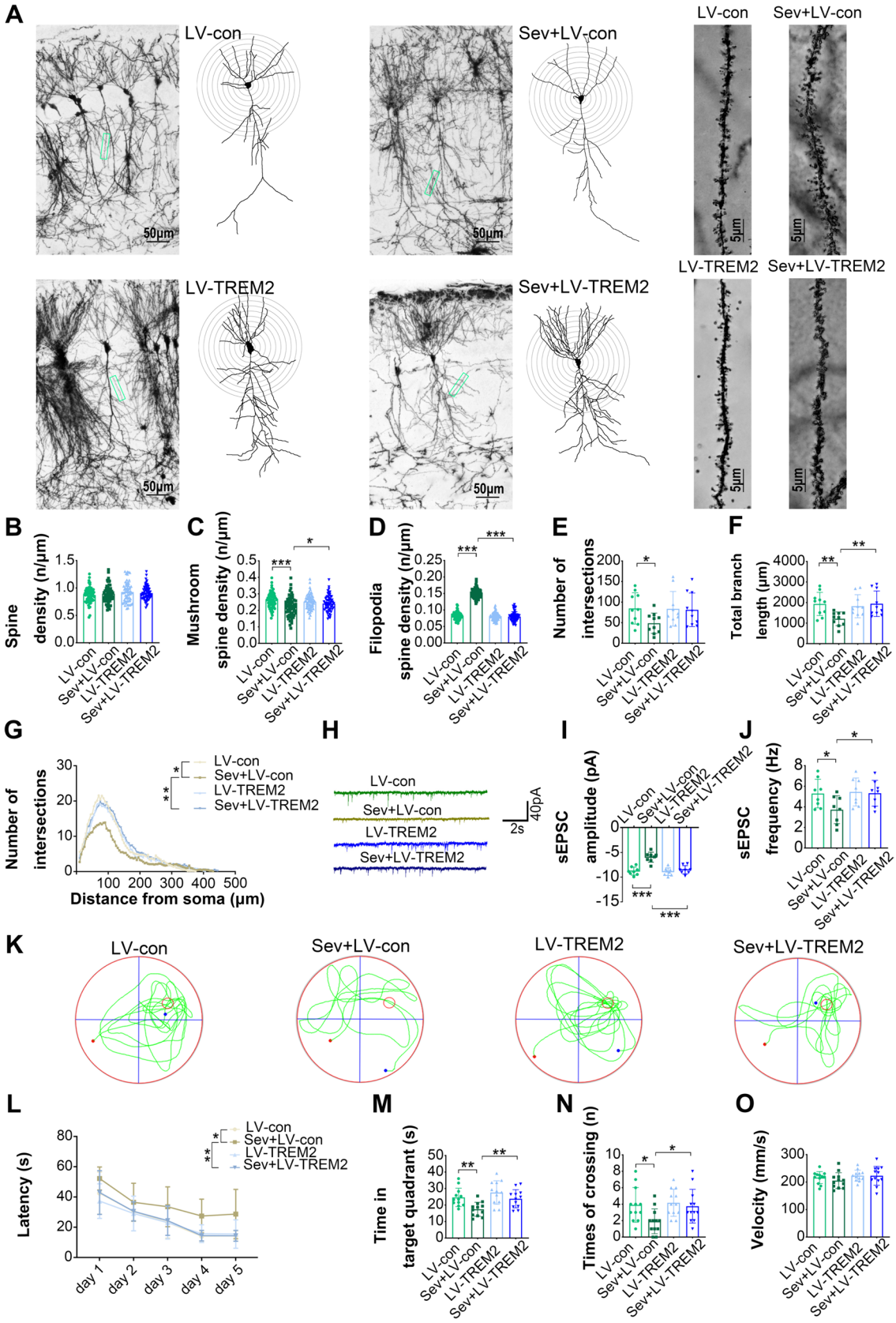
A
LV-con
Sev+LV-con
LV-TREM2
Sev+LV-TREM2
50μm
5μm
B
Spine density (n/μm)
C
Mushroom spine density (n/μm)
D
Filopodia spine density (n/μm)
E
Number of intersections
F
Total branch length (μm)
G
Number of intersections
Distance from soma (μm)
H
40pA
2s
I
sEPSC amplitude (pA)
J
sEPSC frequency (Hz)
K
L
Latency (s)
day 1
day 2
day 3
day 4
day 5
M
Time in target quadrant (s)
N
Times of crossing (n)
O
Velocity (mm/s)

◂**Fig. 6** Overexpression of TREM2 rescued sevoflurane-induced morphological abnormalities of hippocampal CA1 pyramidal neurons and ameliorated cognitive impairment. **A** Representative Golgi staining images of CA1 pyramidal neurons and dendritic spines in the LV-con and LV-TREM2 mice with or without sevoflurane treatment. **B–D** The density of total, mushroom, and filopodia spines in the 4 groups (n = 60). **E–F** Number of intersections and total branch length of dendrites in the 4 groups (n = 10). **G** Number of intersections along the dendrites at all distances from the soma of CA1 neurons in the 4 groups (n = 10, F = 3.857, P = 0.017). **H** Representative traces of sEPSCs of whole-cell patch-clamp recordings from CA1 neurons in the 4 groups. **I–J** Quantification of sEPSCs amplitude and frequency in the 4 groups (n = 8). **K** Representative moving traces of the 4 groups on the testing stage of MWM. **L** Escape latency of the 4 groups in the 5 days on the training stage of MWM (n = 12, F = 7.593, $P < 0.001$). **M–O** Time spent in the fourth quadrant, platform-crossing times, and swimming speed of the 4 groups on the testing stage of MWM (n = 12). Data are mean ± SD. One-way analysis of variance followed by Tukey post hoc test, or two-way repeated-measure analysis of variance followed by Bonferroni post hoc test. $^{*}P < 0.05$, $^{**}P < 0.01$, $^{***}P < 0.001$. MWM, Morris water maze; sEPSC, spontaneous excitatory postsynaptic current.

connections are formed in dendritic spines. Spinal shrinkage and elimination are essential for the development of neural circuits. Morphological changes in the dendritic spines in the early stages affect the formation and fine-tuning of neural circuits. The analysis of spine morphology provides an important indication of synaptic function. Most spines have constricted necks and are either mushroom-shaped with heads exceeding 0.6 microns in diameter or thin-shaped with smaller heads [27]. Mushroom spines are stable and predominate in the mature central nervous system. Filopodia spines have immature morphology with pointy tips and highly motile spinal heads. During the first postnatal week, filopodia are abundant in pyramidal neurons. Spine density increases after 2 weeks, and the spines attain a mature morphology with bulbous heads, similar to those seen in adult mice. Studies have suggested that exposing rodent pups to anaesthetics increases the density of dendritic spines and synapses in several brain areas [17, 28]. These effects may persist for weeks, affect the formation of functional synapses, and lead to stunted dendritic growth.

Our results showed that multiple sevoflurane exposures increased the density of filopodia and total spines on PNDs 10 and 20. On PND 37, more filopodia spines and fewer mushroom spines were observed in the sevoflurane group than in the control group. Several possible mechanisms underlie this phenomenon. Actin filaments gather in the spine necks, and their polymerization-depolymerization states modulate the shape of the spine head. Volatile anaesthetics induced concentration-dependent inhibition of N-methyl-D-aspartate (NMDA)-gated currents, produced approximately 30% inhibition at anaesthetic concentrations, and reduced calcium influx [29]. The downstream Ca^{2+}-dependent activation of calcineurin (protein phosphatase 2B) caused alterations in actin states and morphological changes in spines [30]. Under this condition, excess dendritic spines induced upregulation of eat-me signals and recruited microglia expressing TREM2 to promote phagocytosis of dendritic spines.

We found that the intersection and total dendritic length of the CA1 neurons significantly decreased after sevoflurane exposure. Patch-clamp assays confirmed that the morphological changes in neurons resulted in altered neuronal excitability. Decreased synaptic transmission is closely associated with cognitive impairment. Neurobehavioral impairment induced by sevoflurane was aggravated after the downregulation of TREM2, whereas TREM2 upregulation alleviated these impairments. This indicated that TREM2 promotes the anti-neurotoxic function of microglia in the CA1 region. These results confirm our conjecture that sevoflurane causes alterations in dendritic spines, thereby affecting dendrite formation and resulting in cognitive dysfunction.

Previous in vitro experiments have shown that sevoflurane exerted a direct impact on microglial cells by promoting M1 polarization, suppressing M2 polarization, and stimulating the generation of inflammatory mediators [31–33]. It has also been reported that sevoflurane may inhibit the phagocytosis of microglial cells 24 hours after exposure [34]. Given that our study focused on investigating the influence of neonatal exposure to sevoflurane on adolescent mice, the observational timeframe was considerably extended, presenting a substantial disparity from those in cell experiments. Additionally, exposure to sevoflurane-induced alterations in the environment within the central nervous system of animals, and microglial cells were influenced by neurons and other cells. As a result, in vitro cell experiments cannot adequately imitate the state of microglial cells at 27 days after sevoflurane exposure in mice of our study.

Research has suggested that Iba1 is not a specific marker for microglia but also infiltrated monocytes [35]. Apart from using Iba1 for those identification of microglia, we performed experiments using the microglia-restricted marker, TMEM119 [25]. We showed a significant co-localization of $Iba1^{+}$ cells and $TMEM119^{+}$ cells, and TREM2 was almost exclusively expressed on microglial cells. Therefore, we confirmed the specific cell type of microglia by using both Iba1 and TMEM119. We believed that microglia played a predominant role in our model. The question of whether mononuclear cells were involved in this model remains an intriguing topic for future investigation.

There are several limitations in our study. First, we focused on the role of TREM2 in microglial pruning of dendritic spines in CA1 neurons during sevoflurane-induced developmental neurotoxicity in mice. Abnormal dendritic spine elevation occurred before the upregulation of TREM2 expression. Further investigations are required to elucidate the specific mechanism, particularly the upstream signaling pathways. Second, we used *Trem2* heterozygous KO

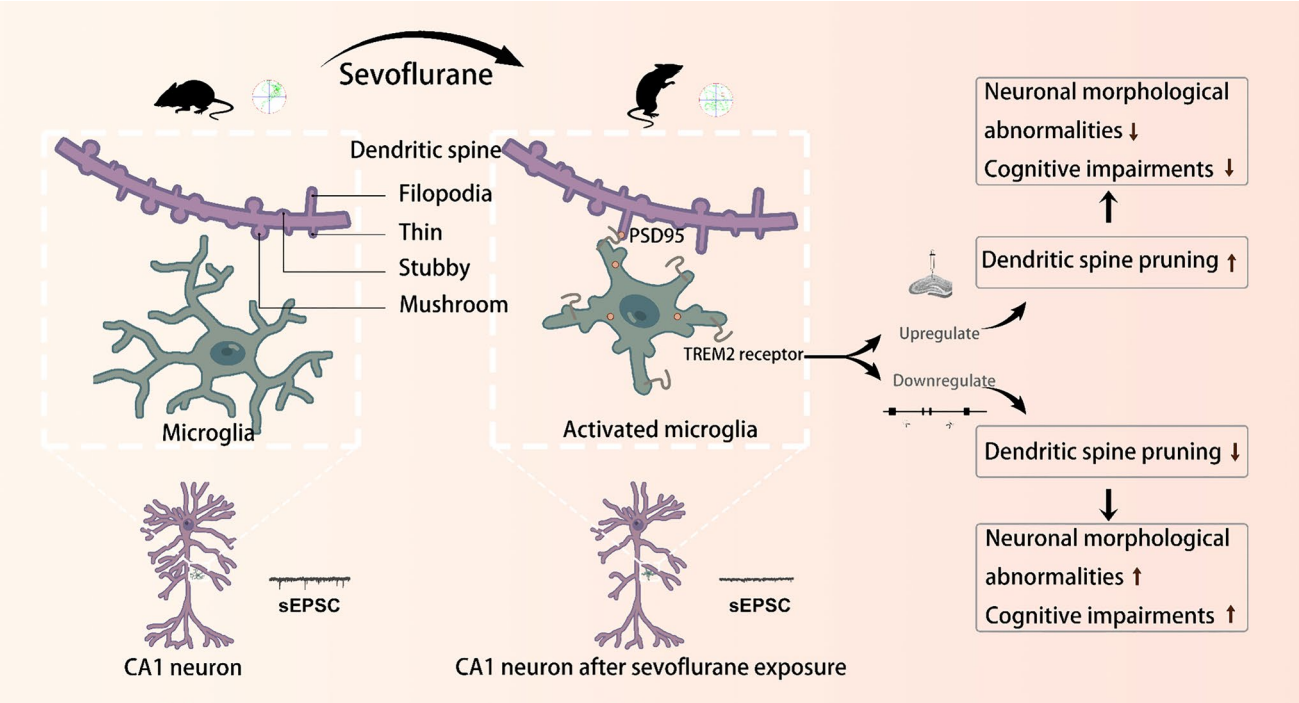

Fig. 7 Schematic mechanism of TREM2 enhancing microglial pruning of dendritic spines in CA1 region to reduce sevoflurane-induced developmental neurotoxicity. The upregulation of TREM2 enhanced microglia-mediated pruning of dendritic spines and rescued sevoflurane-induced neuronal morphological abnormalities and cognitive dysfunction.

mice. Although TREM2 genetic knockdown significantly decreased dendritic spine pruning, it only partially aggravated neuronal morphological abnormalities and cognitive impairments in sevoflurane-treated mice. It is possible that the remaining expression of TREM2 in the heterozygous mice still exerted protection against these declines. According to the literature, homozygous TREM2 knockout mice exhibited an increased number of dendritic spines of neurons [10]. As such, it would lead to a non-comparable baseline spine density which was deemed not suitable to fit our model. Therefore, we chose heterozygous mice to minimize the impact of complete TREM2 gene knockout on dendritic spines (as shown in Figure 2C). Third, downregulation of TREM2 protein expression occurred before sevoflurane exposure. Although previous evidence and our experiment indicate that *Trem2*$^{-/+}$ mice do not display learning and memory defects in behavioral tests, the effects of the genetic knockdown of TREM2 on brain development remain unclear. Finally, the number of animals per analysis was relatively limited; therefore, replication of our results is required in future studies.

In conclusion, this study demonstrated the protective role of TREM2 against sevoflurane-induced developmental neurotoxicity in mice by facilitating the microglia-mediated pruning of dendritic spines in CA1 neurons (Fig. 7). Thus, TREM2 may be a potential therapeutic target in the prevention of AIDN. Further studies on the molecular cascades underlying dendritic spine changes and TREM2 upregulation are warranted.

Acknowledgments This work was supported by the National Natural Science Foundation of China (82072130 and 82001126), Key Medical Research Projects in Jiangsu Province (ZD2022021), Six Talent Peaks Project in Jiangsu Province (WSN-022), Suzhou Clinical Medical Center for Anaesthesiology (Szlcyxzxj202102), Jiangsu Medical Association Anaesthesia Research Project (SYH-32021-0036 (2021031)), Suzhou Medical Health Science and Technology Innovation Project (SKY2022136), Jiangsu Provincial Colleges of Natural Science General Program (22KJD320002), Health Talent Plan Project in Suzhou (GSWS2022007), and Gusu Health Talent Project of Soochow (GSWS2021062).

Data availability The datasets generated during and/or analyzed during the current study are available from the corresponding author upon reasonable request.

Conflict of interest All authors declare that there are no conflicts of interest.

References

1. Nair AS, Pulipaka K, Rayani BK. Anesthetic-induced developmental neurotoxicity: Causes, prospective studies and possible interventions. Med Gas Res 2017, 7: 224–225.

2. Sun L. Early childhood general anaesthesia exposure and neurocognitive development. Br J Anaesth 2010, 105: i61–i68.
3. Shen X, Dong Y, Xu Z, Wang H, Miao C, Soriano SG. Selective anesthesia-induced neuroinflammation in developing mouse brain and cognitive impairment. Anesthesiology 2013, 118: 502–515.
4. Useinovic N, Maksimovic S, Near M, Quillinan N, Jevtovic-Todorovic V. Do we have viable protective strategies against anesthesia-induced developmental neurotoxicity? Int J Mol Sci 2022, 23: 1128.
5. Davidson AJ, Disma N, de Graaff JC, Withington DE, Dorris L, Bell G, *et al*. Neurodevelopmental outcome at 2 years of age after general anaesthesia and awake-regional anaesthesia in infancy (GAS): An international multicentre, randomised controlled trial. Lancet 2016, 387: 239–250.
6. Li G, Du JE, Wang L, Shi X. Developmental neurotoxicity in the context of multiple sevoflurane exposures: Potential role of histone deacetylase 6. Neurotoxicol Teratol 2019, 74: 106813.
7. Kong FJ, Ma LL, Hu WW, Wang WN, Lu HS, Chen SP. Fetal exposure to high isoflurane concentration induces postnatal memory and learning deficits in rats. Biochem Pharmacol 2012, 84: 558–563.
8. Kettenmann H, Hanisch UK, Noda M, Verkhratsky A. Physiology of microglia. Physiol Rev 2011, 91: 461–553.
9. Kim HJ, Cho MH, Shim WH, Kim JK, Jeon EY, Kim DH, *et al*. Deficient autophagy in microglia impairs synaptic pruning and causes social behavioral defects. Mol Psychiatry 2017, 22: 1576–1584.
10. Filipello F, Morini R, Corradini I, Zerbi V, Canzi A, Michalski B, *et al*. The microglial innate immune receptor TREM2 is required for synapse elimination and normal brain connectivity. Immunity 2018, 48: 979-991.e8.
11. Song SY, Meng XW, Xia Z, Liu H, Zhang J, Chen QC, *et al*. Cognitive impairment and transcriptomic profile in hippocampus of young mice after multiple neonatal exposures to sevoflurane. Aging 2019, 11: 8386–8417.
12. Johnson MZ, Crowley PD, Foley AG, Xue C, Connolly C, Gallagher HC, *et al*. Effect of perioperative lidocaine on metastasis after sevoflurane or ketamine-xylazine anaesthesia for breast tumour resection in a murine model. Br J Anaesth 2018, 121: 76–85.
13. Savage JC, Picard K, González-Ibáñez F, Tremblay MÈ. A brief history of microglial ultrastructure: Distinctive features, phenotypes, and functions discovered over the past 60 Years by electron microscopy. Front Immunol 2018, 9: 803.
14. Harris KM, Kater SB. Dendritic spines: Cellular specializations imparting both stability and flexibility to synaptic function. Annu Rev Neurosci 1994, 17: 341–371.
15. Wieshahn GP, Hyde JE, Hearst JE. The photoaddition of trimethylpsoralen to *Drosophila melanogaster* nuclei: A probe for chromatin substructure. Biochemistry 1977, 16: 925–932.
16. Petit TL, LeBoutillier JC, Gregorio A, Libstug H. The pattern of dendritic development in the cerebral cortex of the rat. Brain Res 1988, 469: 209–219.
17. Briner A, De Roo M, Dayer A, Muller D, Habre W, Vutskits L. Volatile anesthetics rapidly increase dendritic spine density in the rat medial prefrontal cortex during synaptogenesis. Anesthesiology 2010, 112: 546–556.
18. Paolicelli RC, Bolasco G, Pagani F, Maggi L, Scianni M, Panzanelli P, *et al*. Synaptic pruning by microglia is necessary for normal brain development. Science 2011, 333: 1456–1458.
19. Werneburg GT, Nguyen A, Henderson NS, Rackley RR, Shoskes DA, Le Sueur AL, *et al*. The natural history and composition of urinary catheter biofilms: Early uropathogen colonization with intraluminal and distal predominance. J Urol 2020, 203: 357–364.
20. Vasek MJ, Garber C, Dorsey D, Durrant DM, Bollman B, Soung A, *et al*. A complement-microglial axis drives synapse loss during virus-induced memory impairment. Nature 2016, 534: 538–543.
21. Deczkowska A, Weiner A, Amit I. The physiology, pathology, and potential therapeutic applications of the TREM2 signaling pathway. Cell 2020, 181: 1207–1217.
22. Qu S, Hu S, Xu H, Wu Y, Ming S, Zhan X, *et al*. TREM-2 drives development of multiple sclerosis by promoting pathogenic Th17 polarization. Neurosci Bull 2024, 40: 17–34.
23. Schafer DP, Lehrman EK, Kautzman AG, Koyama R, Mardinly AR, Yamasaki R, *et al*. Microglia sculpt postnatal neural circuits in an activity and complement-dependent manner. Neuron 2012, 74: 691–705.
24. Hsieh CL, Koike M, Spusta SC, Niemi EC, Yenari M, Nakamura MC, *et al*. A role for TREM2 ligands in the phagocytosis of apoptotic neuronal cells by microglia. J Neurochem 2009, 109: 1144–1156.
25. Scott-Hewitt N, Perrucci F, Morini R, Erreni M, Mahoney M, Witkowska A, *et al*. Local externalization of phosphatidylserine mediates developmental synaptic pruning by microglia. EMBO J 2020, 39: e105380.
26. Schikorski T, Stevens CF. Morphological correlates of functionally defined synaptic vesicle populations. Nat Neurosci 2001, 4: 391–395.
27. Harris KM, Jensen FE, Tsao B. Three-dimensional structure of dendritic spines and synapses in rat hippocampus (CA1) at postnatal day 15 and adult ages: Implications for the maturation of synaptic physiology and long-term potentiation. J Neurosci 1992, 12: 2685–2705.
28. de Roo M, Klauser P, Briner A, Nikonenko I, Mendez P, Dayer A, *et al*. Anesthetics rapidly promote synaptogenesis during a critical period of brain development. PLoS One 2009, 4: e7043.
29. Criswell HE, Ming Z, Pleasant N, Griffith BL, Mueller RA, Breese GR. Macrokinetic analysis of blockade of NMDA-gated currents by substituted alcohols, alkanes and ethers. Brain Res 2004, 1015: 107–113.
30. Stein IS, Zito K. Dendritic spine elimination: Molecular mechanisms and implications. Neuroscientist 2019, 25: 27–47.
31. Pei Z, Wang S, Li Q. Sevoflurane suppresses microglial M2 polarization. Neurosci Lett 2017, 655: 160–165.
32. Chen H, Chu H, Jiang Q, Wang C, Tian Y. Irf6 participates in sevoflurane-induced perioperative neurocognitive disorder via modulating M2, but not M1 polarization of microglia. Brain Res Bull 2021, 177: 1–11.
33. Yu X, Zhang F, Shi J. Effect of sevoflurane treatment on microglia activation NF-kB and MAPK activities. Immunobiology 2019, 224: 638–644.
34. Zhu R, Zeng S, Li N, Fu N, Wang Y, Miao M, *et al*. Sevoflurane exposure induces neurotoxicity by regulating mitochondrial function of microglia due to NAD insufficiency. Front Cell Neurosci 2022, 16: 914957.
35. Kenkhuis B, Somarakis A, Kleindouwel LRT, van Roon-Mom WMC, Höllt T, van der Weerd L. Co-expression patterns of microglia markers Iba1, TMEM119 and P2RY12 in Alzheimer's disease. Neurobiol Dis 2022, 167: 105684.